Efficient Classification of Optical Modulation Formats Based on Singular Value Decomposition and Radon Transformation

Rania A. Eltaieb, Ahmed E. A. Farghal, HossamEl-din H. Ahmed, Waddah S. Saif, Amr Ragheb, Saleh A. Alshebeili, Hossam M. H. Shalaby, *Senior Member, IEEE, Senior Member, OSA*, and Fathi E. Abd El-Samie

***Abstract*—Two schemes for blind optical modulation format identification (MFI), based on the singular value decomposition (SVD) and Radon transform (RT) of the constellation diagrams, are proposed. Constellation diagrams are obtained at optical signal-to-noise ratios (OSNRs) ranging from 2 to 30 dB for eight different modulation formats as images. The first scheme depends on the utilization of feature vectors composed of the singular values (SVs) of the obtained images, while the second scheme is based on applying the RT and then getting the SVs. Different classifiers are used and compared for the MFI task. The effect of varying the number of samples on the accuracy of the classifiers is studied for each modulation format. Simulation and experimental setups have been provided to study the efficiency of the two schemes at high bit rates for three dual-polarized modulation formats. A decimation approach for the constellation diagrams is suggested to reduce the SVD complexity, while maintaining high classification accuracy. The obtained results reveal that the proposed schemes can accurately be used to identify the optical modulation format blindly with classification rates up to 100% even at low OSNR values of 10 dBs.**

***Index Terms*—Coherent detection, intelligent receiver, machine learning classifiers, modulation format identification, radon transform, singular value decomposition.**

Manuscript received May 29, 2019; revised July 21, 2019, August 28, 2019, and September 13, 2019; accepted October 8, 2019. Date of publication October 14, 2019; date of current version February 1, 2020. This work was supported by King Saud University through the Researchers Supporting Project number (RSP-2019/46). *(Corresponding author: Rania A. Eltaieb.)*

R. A. Eltaieb, H. H. Ahmed, and F. E. Abd El-Samie are with the Department of Electronics and Electrical Communications Engineering, Faculty of Electronics Engineering, Menoufia University, Menouf 32952, Egypt (e-mail: rania-antar@el-eng.menofia.edu.eg; hhossamkh@yahoo.com; fathi_sayed@yahoo.com).

A. E. A. Farghal is with Electrical Engineering Department, Faculty of Engineering, Sohag University, Sohag 82524, Egypt (e-mail: ahmed.farghal@eng.sohag.edu.eg).

W. S. Saif and S. A. Alshebeili are with the Department of Electrical Engineering, King Saud University, Riyadh 11421, Saudi Arabia, and also with KACST-TIC in Radio Frequency and Photonics for the e-Society, King Saud University, Riyadh 11421, Saudi Arabia (e-mail: wsaif@ksu.edu.sa; dsaleh@ksu.edu.sa).

A. Ragheb is with KACST-TIC in Radio Frequency and Photonics for the e-Society, King Saud University, Riyadh 11421, Saudi Arabia (e-mail: aragheb@ksu.edu.sa).

H. M. H. Shalaby is with Electrical Engineering Department, Alexandria University, Alexandria 21544, Egypt, and also with the Department of Electronics and Communications Engineering, Egypt-Japan University of Science and Technology, Alexandria 21934, Egypt (e-mail: shalaby@ieee.org).

Color versions of one or more of the figures in this article are available online at http://ieeexplore.ieee.org.

Digital Object Identifier 10.1109/JLT.2019.2947154

I. Introduction

IN FLEXIBLE and adaptive optical communication systems, data rates and modulation formats are changed depending on user demands and channel conditions [1]. Additionally, enhancement of spectral efficiency is required. This can be achieved by removing the end-to-end handshaking information between the transmitter and the receiver. Therefore, identifying the different modulation formats at the receiver has become an issue that needs to be addressed. In this context, intelligent coherent receivers with blind modulation format identification (MFI) are exploited to solve this problem [2].

Several trends for blind optical MFI have been presented in the literature. Bilal *et al.* [3] presented an approach for optical modulation classification based on the peak-to-average power ratio (PAPR) of the received data samples. They relied on the fact that each format has different PAPR values at definite OSNRs. This approach achieves high accuracy, but with prior knowledge and large values of the OSNR. Adles *et al.* [4] presented another approach based on the obtained histograms of the electric field distributions. This approach provides high classification rates, but it is complex in the computation process. Liu *et al.* [5] proposed a method of using the power distribution of the received signals for MFI. Although this method succeeded in the recognition, different thresholds are required to be adjusted for the parameters of interest.

Recently, machine learning technology has been utilized in optical communication systems in several fields including MFI [6]. Khan *et al.* [7], [8] proposed a method of using the amplitude histograms obtained from the constellation diagrams, and then they used the artificial neural networks (ANNs) [7] and the deep neural networks (DNNs) [8] for MFI. These two ways provide high accuracy but non of them could identify the higher orders of the phase-shift keying (PSK) formats due to the similarity of their amplitude histograms. Bo *et al.* [9] used the binary images resulting from the Voronoi diagrams for MFI. Although high accuracy is achieved, a large number of samples is required for identifying 16-QAM modulation. Furthermore, the constellation diagrams [10], [11] and eye diagrams [12] have been used with convolutional neural networks (CNNs) for MFI.

In this paper, two blind optical MFI schemes based on SVD of the constellation diagrams and their RTs are presented. A

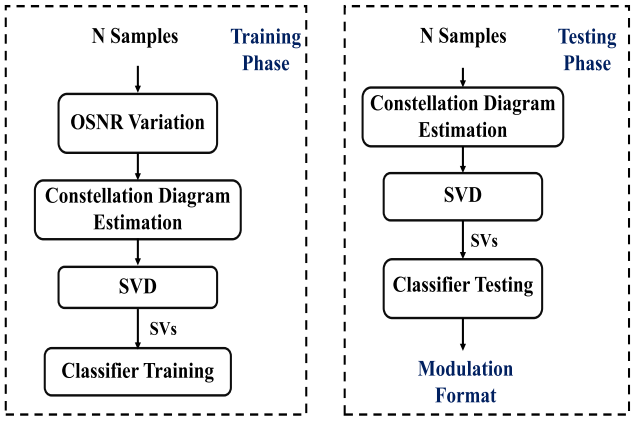

Fig. 1. Block diagram of the proposed SVD scheme.

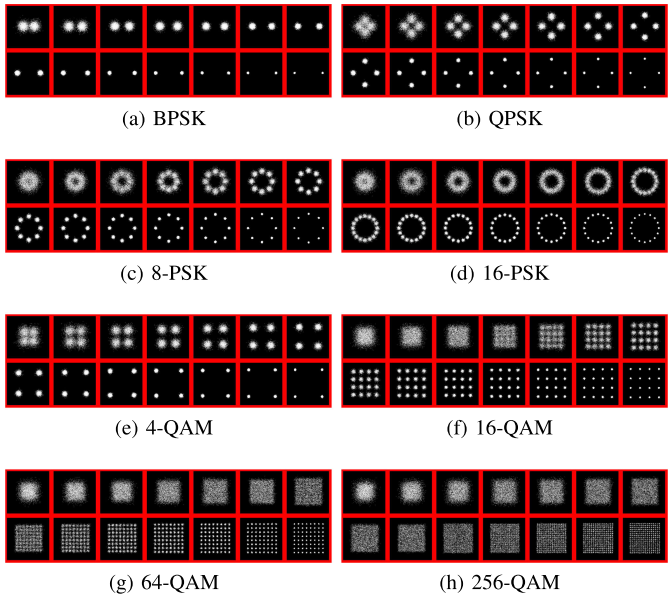

Fig. 2. Samples of the used constellation diagrams for all modulation formats. The OSNR changes from left to right in the range of 4 to 30 dB with 2-dB steps.

coherent optical receiver is adopted to implement eight modulation formats (4/16/64/256-QAM and B/Q/8/16-PSK) with a definite OSNR range and several numbers of samples. The SVs of these diagrams are dependent on the type of the modulation format. High identification rates among all formats are obtained even at low OSNR values and small numbers of samples. Complexity reduction is tested through decimation of constellation diagrams for dual-polarized modulation formats. State of polarization and phase noise effects are considered on five dual-polarized modulation formats for the MFI task. Furthermore, a comparison study between the proposed MFI schemes and the traditional MFI schemes is presented considering both the number of samples and the OSNR as metrics.

The proposal of adopting SVD for MFI is based on the following advantages [13]:

- The constellation diagrams and their shifted or rotated versions have the same SVs.
- The SVs have a good stability even when slight variations affect the constellation diagrams. These slight variations may appear due to channel degradation effects.

The rest of this paper is organized as follows. The proposed SVD-based MFI is described in Section II. Section III is devoted to the mathematical representation of the RT for optical MFI. The effects of phase noise and state of polarization on MFI task are presented in Section IV. Section V provides a complexity reduction approach for the classification process based on constellation diagram decimation prior to estimation of the SVD. In Section VI, the simulation setup is presented. The experimental setup is provided in Section VII. The numerical results are presented in Section VIII. Finally, the conclusion is given in Section IX.

II. Proposed SVD MFI Scheme

Fig. 1 shows the block diagram of the proposed SVD scheme for optical MFI. As shown in this figure, there is a need for both training and testing phases. In both phases, the number of used samples is to be determined first. Next, constellation diagram estimation is performed in the used OSNR range. Finally, the features are extracted and machine learning classifiers are used.

An adaptive optical modulation system is adopted comprising 8 modulation formats (4/16/64/256-QAM and B/Q/8/16-PSK). The adaptation among modulation orders is dependent upon the required data rates and OSNR limitations. The MFI step is performed at the receiver before the DSP processes that are modulation format dependent, like carrier phase recovery and adaptive equalization.

The MFI is performed depending on the SVDs of the constellation diagrams. So, there is a need to regularly estimate the constellation diagrams from finite lengths of the received data. The constellation diagram is used as an image. Specifically, it is captured as a color image with a pixel size of 656 $\times$ 656 in bmp format. This image is then converted to a gray-scale image for the purpose of reducing the computational load. The SVD of the gray-scale image produces three matrices, namely $\mathbf{U}$, $\mathbf{S}$ and $\mathbf{V}$, as follows [13]:

$$\mathbf{I} = \mathbf{U}\mathbf{S}\mathbf{V}^{T}, \tag{1}$$

where $\mathbf{U}$ and $\mathbf{V}$ are the left and right singular vectors of the matrix $\mathbf{I}$ representing the constellation diagram, respectively, and T denotes the transpose. The diagonal elements of the matrix $\mathbf{S}$ constitute the feature vector.

In this scheme, training is performed on samples of constellation diagrams of each modulation format acquired at different OSNR levels. The diversity of OSNRs used in the training phase allows OSNR-independent MFI. The testing phase begins with a similar SVD process to extract the features.

Fig. 2 shows samples of the obtained constellation diagrams at OSNRs ranging from 4 to 30 dB with 6000 samples. Different types of classifiers are used, namely support vector machine (SVM), K-nearest neighbor (KNN), and decision tree (DT) [2].

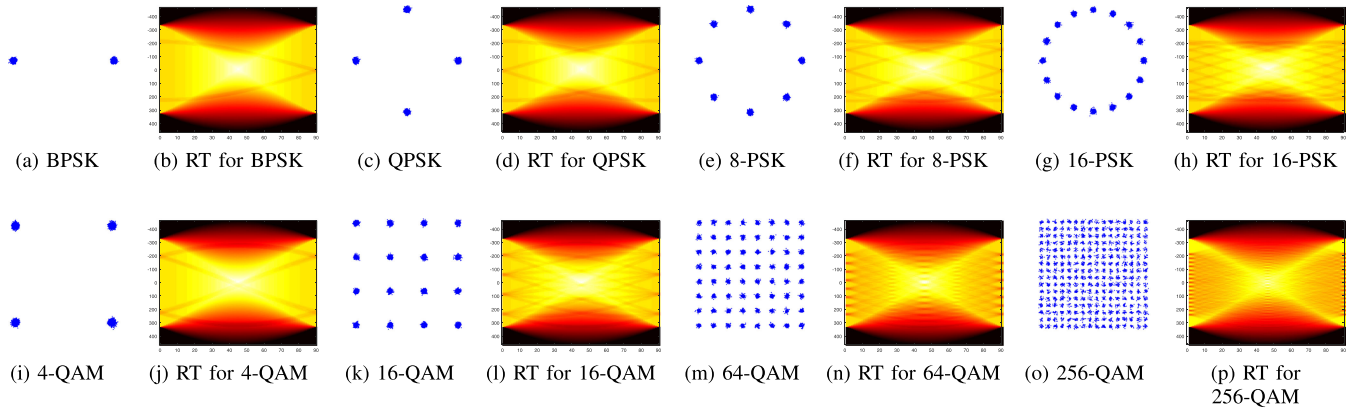

Fig. 3. Samples of the used constellation diagrams and their RTs for all modulation formats with an OSNR of 30 dBs.

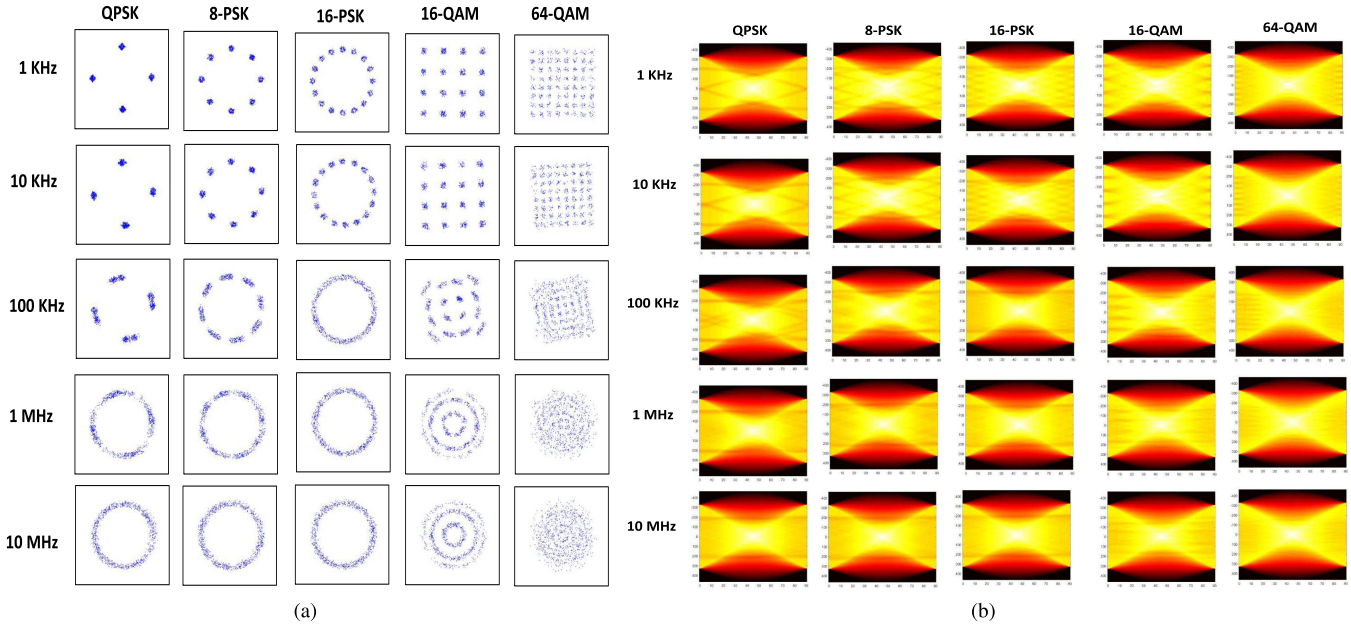

Fig. 4. Samples of the constellation diagrams and their RTs at different PN levels.

III. Radon-Based MFI Scheme

Due to the characteristics of the RT to represent images through different projections, it can be used to give sophisticated representations of constellation diagrams, as shown in Fig. 3.

The RT is estimated by [14]:

$$R(t,\theta) = \int_{-\infty}^{\infty}\int_{-\infty}^{\infty} I(x,y)\delta\left[t - x\cos(\theta) - y\sin(\theta)\right]\, dxdy, \tag{2}$$

where $I(x,y)$ is the constellation diagram image, x and y represent the coordinate positions, $R(t,\theta)$ is the RT image, t is the normal distance from the origin to the line of projection, θ is the projection angle, which is the angle between the normal distance and the horizontal axis of an image and $\delta(\cdot)$ is the Dirac delta function. The RT is determined by the summation of all values in the matrix, taking into consideration the angle of projection. In this paper, the projection angle is taken from 0° to 90° due to similarity properties of the RT. The proposed scheme depends on performing the RT and SVD for feature extraction. This hybrid scheme guarantees robustness to impairment effects.

Each constellation diagram has a definite number of points at definite positions depending on the type of the modulation format. These points are mapped to more distinctive curved lines in the RT image. These lines help in enhancing the identification accuracy.

IV. Phase Noise and State of Polarization Effects

Fig. 4(a) illustrates the constellation diagrams of five types of modulation formats considered in this paper at different levels of phase noise (PN). It is clear that the PN leads to some sort of non-uniform rotation [15]. After 1 MHz PN, spreading of constellation diagram points becomes more pronounced. This effect leads to serious degradations in the constellation diagrams of QPSK, 8-PSK and 16-PSK. Traditional pattern recognition schemes may fail in this scenario. Even with the spreading

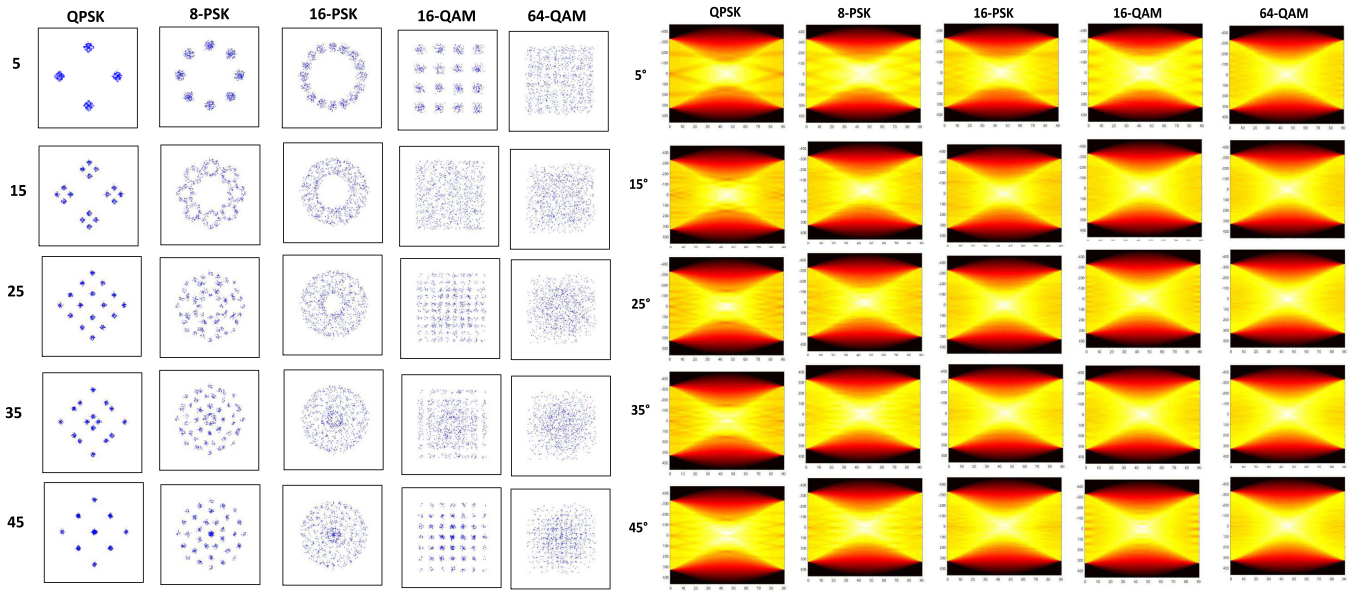

Fig. 5. Samples of the constellation diagrams and their RTs at different SoP values.

of constellation diagram points at high PN levels in the form of a continuous circle, there exist some regions on the circle circumference at which density of points is high, while the rest of the circumference is of low-density, which can be interpreted as noise added to the original constellation diagram. The effect of this noise on the SVs of a constellation diagram is expected to be less than the effect on the constellation diagram itself.

The RTs of the constellation diagrams in Fig. 4(a) are shown in Fig. 4(b). It is clear that even with high PN levels, the pattern in the RT corresponding to a certain constellation diagram is preserved to a large extent due to the robustness of the RT to noise-like changes in the original constellation diagram image. Application of the SVD and extraction of the SVs as features from the RT with an efficient classifier are expected to yield high classification accuracy.

Another important factor that affects the performance of the optical communication system is the state of polarization (SoP) that leads to polarization cross-talk [16]. Fig. 5(a) shows samples of the constellation diagrams for five modulation formats at different SoP values. Moreover, the RTs of these constellation diagrams are given in Fig. 5(b). From these diagrams, it is clear that there is a unique signature for each constellation diagram even at high SoP values of 45°. The RT in Fig. 5(b) reveals that the main pattern corresponding to each constellation diagram is still distinguishable for each polarization. So, it is expected that an efficient classifier with the proposed schemes can succeed in the MFI task.

V. Constellation Diagram Decimation for Complexity Reduction

Decimation can be used to reduce the dimensions of the constellation diagram to save the time of computation of the SVD. If the lexicographic ordering of the constellation diagram image is performed to yield a 1-D vector $\mathbf{f}$, the decimated constellation diagram can be estimated as follows:

$$\mathbf{g} = \mathbf{D}\mathbf{f}, \tag{3}$$

where $\mathbf{D}$ is the decimation operator defined as $\mathbf{D} = \mathbf{D}_1 \circledast \mathbf{D}_1$, $\circledast$ is the Kronecker product and $\mathbf{D}_1$ is a 1-D filtering and down-sampling operator for decimation by 2 [17].

$$\mathbf{D}_1 = \frac{1}{2}\begin{bmatrix} 1 & 1 & 0 & 0 & \cdots & 0 & 0 \\ 0 & 0 & 1 & 1 & \cdots & 0 & 0 \\ \vdots & \vdots & \vdots & \vdots & \ddots & \vdots & \vdots \\ 0 & 0 & 0 & 0 & \cdots & 1 & 1 \end{bmatrix} \tag{4}$$

For decimation by 2, the obtained image $g(i,j)$ rearranged from $\boldsymbol{g}$ in 2-D will be of dimensions $m/2 \times n/2$ if the image $f(i,j)$ is of dimensions $m \times n$. The complexity of SVD is of $O(m^2n + n^3)$ [18]. Hence, after decimation, the complexity will be of $O((\frac{m}{2})^2(\frac{n}{2}) + (\frac{n}{2})^3)$.

The complexity will be reduced due to the reduction in constellation diagram size, which will provide less singular values for the classification task. The original constellation diagram is of size 656 × 656. Then, the decimated constellation diagram will be of size 328× 328 and 164 × 164 for decimation by 2 and 4, respectively. The main limitation is to keep the ability to identify the modulation formats even with decimation operation. This process will be investigated by both simulation and experimental results. The effect of reducing the image size on the identification accuracy is studied even at low OSNR and different phase noise levels.

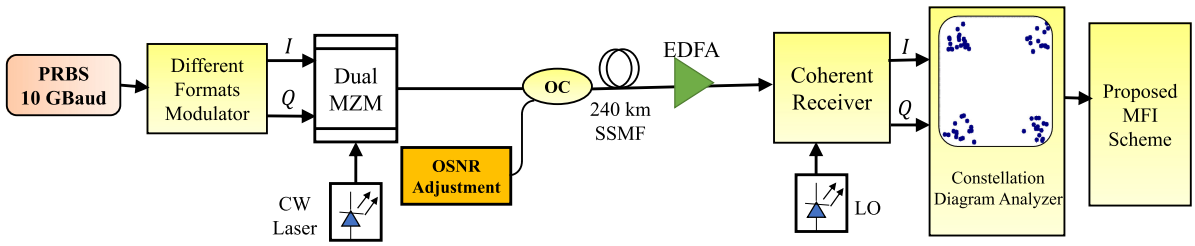

Fig. 6. Simulation system setup for the proposed MFI schemes. CW: continuous wave laser, EDFA: Erbium-doped fiber amplifier, LO: local oscillator, MZM: Mach-Zehnder modulator, OC: optical coupler, PRBS: pseudo-random binary sequence and SSMF: standard single-mode fiber.

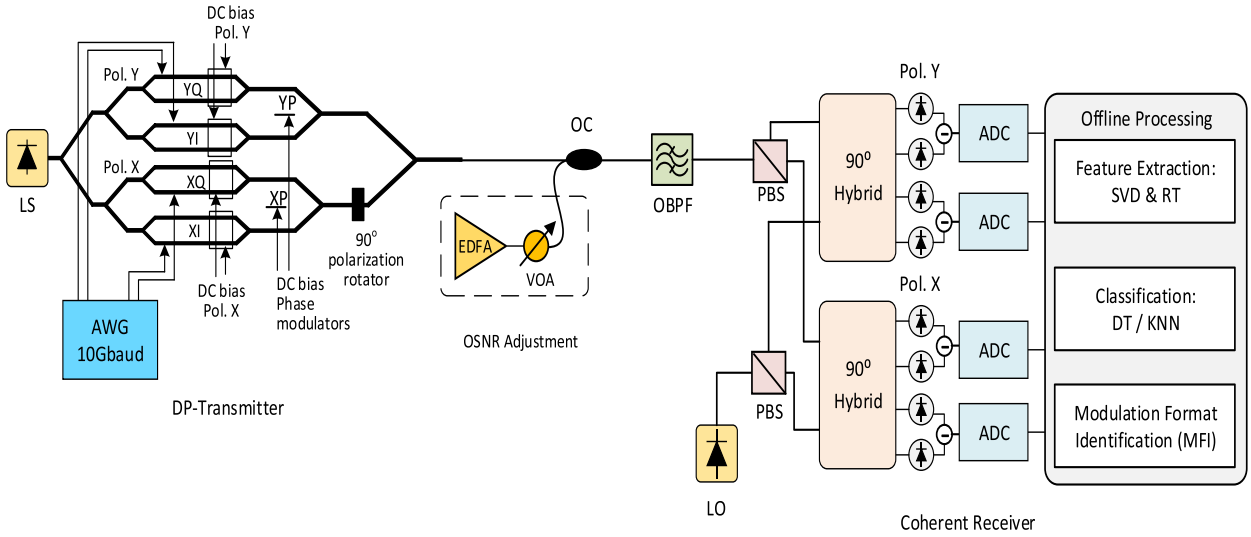

Fig. 7. Experimental setup of the demonstrated optical MFI using the proposed schemes. LS: laser source; AWG: arbitrary waveform generator; XI, XQ, YI, and YQ: Mach Zehnder sub-modulators of X and Y polarization; XP and YP: phase modulator; EDFA: Erbium-doped fiber amplifier; VOA: variable optical attenuator; OC: optical coupler; OBPF: optical band pass filter; LO: local oscillator; PBS: polarization beam splitter; ADC: analog-to-digital converter; SVD: singular value decomposition; RT: Radon transform; DT: decision tree; KNN: K-nearest neighbor.

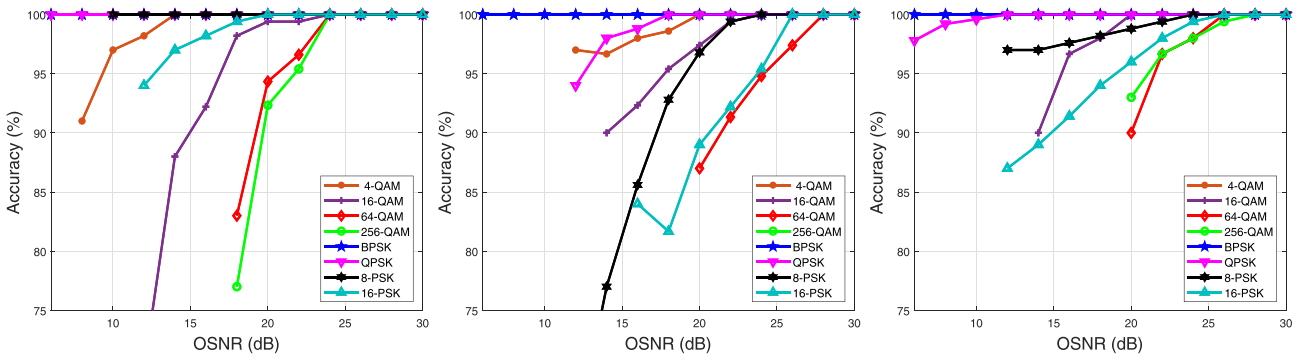

(a) DT classifier (b) SVM classifier (c) KNN classifier

Fig. 8. Accuracy vs. OSNR with 4000 samples for different classifiers.

VI. Simulation Setup

The simulation setup to produce the eight modulation formats (4/16/64/256-QAM and B/Q/8/16-PSK) is implemented using MATLAB. For each modulation format, 15 OSNR values are considered at each determined length of samples. Fifty constellation diagrams are collected at each OSNR for each format.

Moreover, a simulation setup, as shown in Fig. 6, is built based on Opti-System Version 12.0, and five modulation formats are produced and tested: 4-QAM, 16-QAM, QPSK, 8-PSK, and 16-PSK. In all tests, data rate is fixed at 2.5 Gbps. A continuous wave (CW) laser at the wavelength of 1550 nm and linewidth of 100 kHz is used to provide the optical carrier. A pseudo-random binary sequence (PRBS) is used to drive the dual Mach-Zehnder modulator (MZM) to generate the required modulation formats.

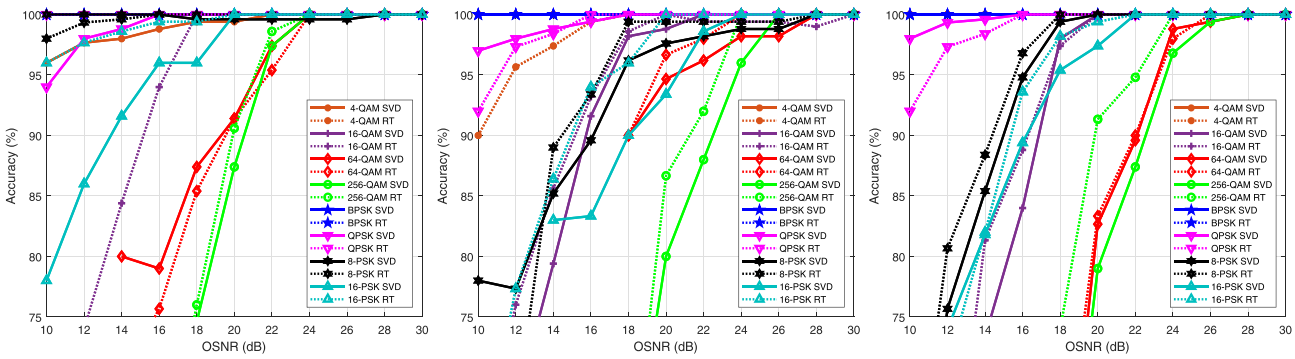

(a) DT classifier (b) SVM classifier (c) KNN classifier

Fig. 9. Comparison between the two proposed schemes with 2000 samples.

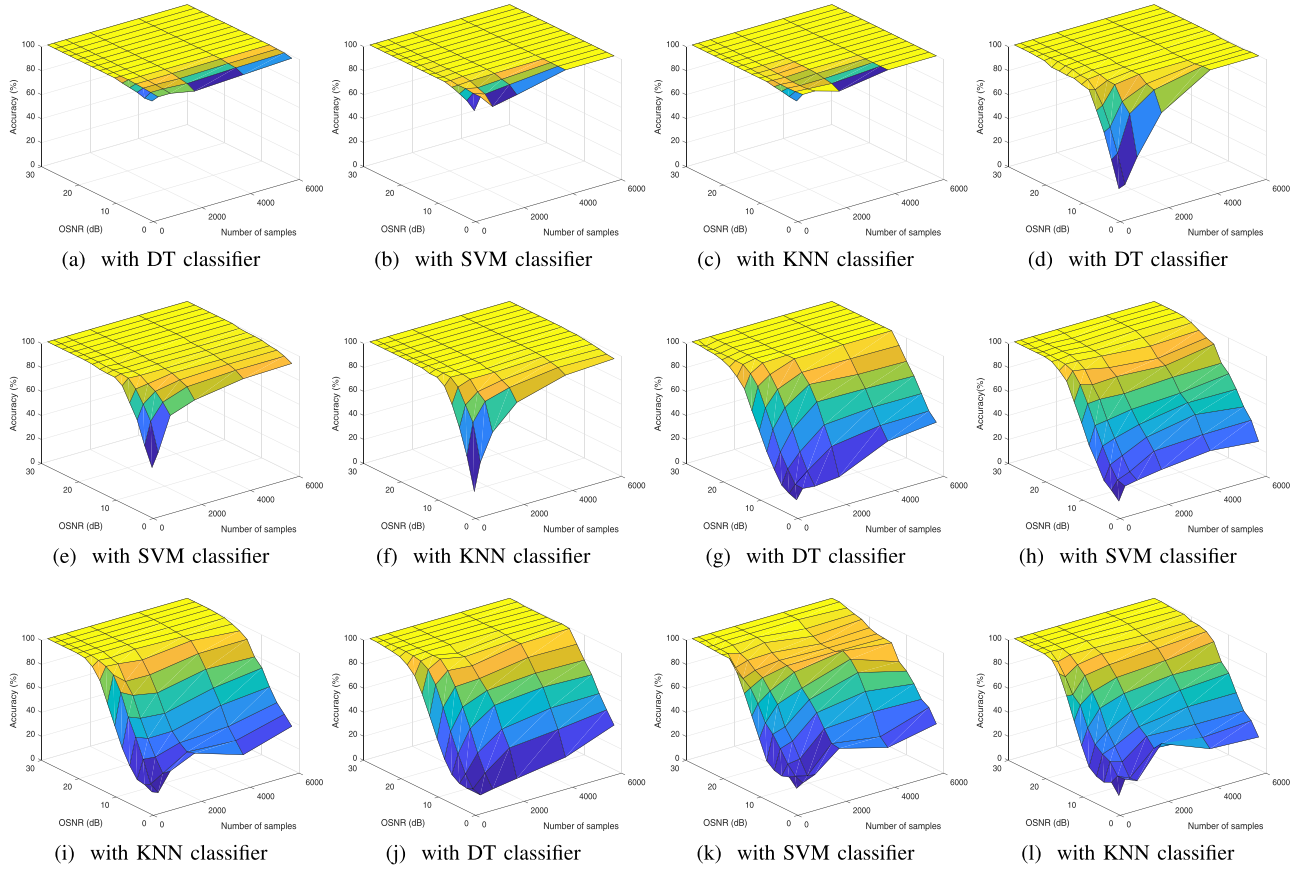

(a) with DT classifier (b) with SVM classifier (c) with KNN classifier (d) with DT classifier

(e) with SVM classifier (f) with KNN classifier (g) with DT classifier (h) with SVM classifier

(i) with KNN classifier (j) with DT classifier (k) with SVM classifier (l) with KNN classifier

Fig. 10. Accuracy vs. number of samples and OSNR values for all PSK modulation formats with the SVD scheme. (a), (b), (c) are for BPSK; (d), (e), (f) are for QPSK; (g), (h), (i) are for 8-PSK; and (j), (k), (l) are for 16-PSK.

The modulated signal is transmitted through a standard single-mode fiber (SSMF) of length 240 km. The OSNR value is controlled to cover the 2 to 30 dB range. An Erbium-doped fiber amplifier (EDFA) is used to completely compensate for the transmission loss. At the receiver side, the signal is passed through the optical filter. A coherent detector, which has balanced photodetection (BPD), is used with a local oscillator (LO). The constellation diagrams have been collected using the constellation diagram analyzer that needs the in-phase (I) and quadrature (Q) components of the incoming signal. Then, the obtained constellation diagrams are processed with the proposed model to extract the dominant features using the SVD. Finally, the classifiers are applied and the accuracy is determined.

The MFI is tested in the presence of PN and SoP effects for five modulation formats (20 Gbps-DP-QPSK, 30 Gbps-DP-8-PSK, 40 Gbps-DP-16-PSK, 40 Gbps-DP-16-QAM and 60 Gbps-DP-64-QAM) at a high level of OSNR of 30 dBs. The PN level is varied from 1 kHz to 10 MHz and the SoP value is varied from

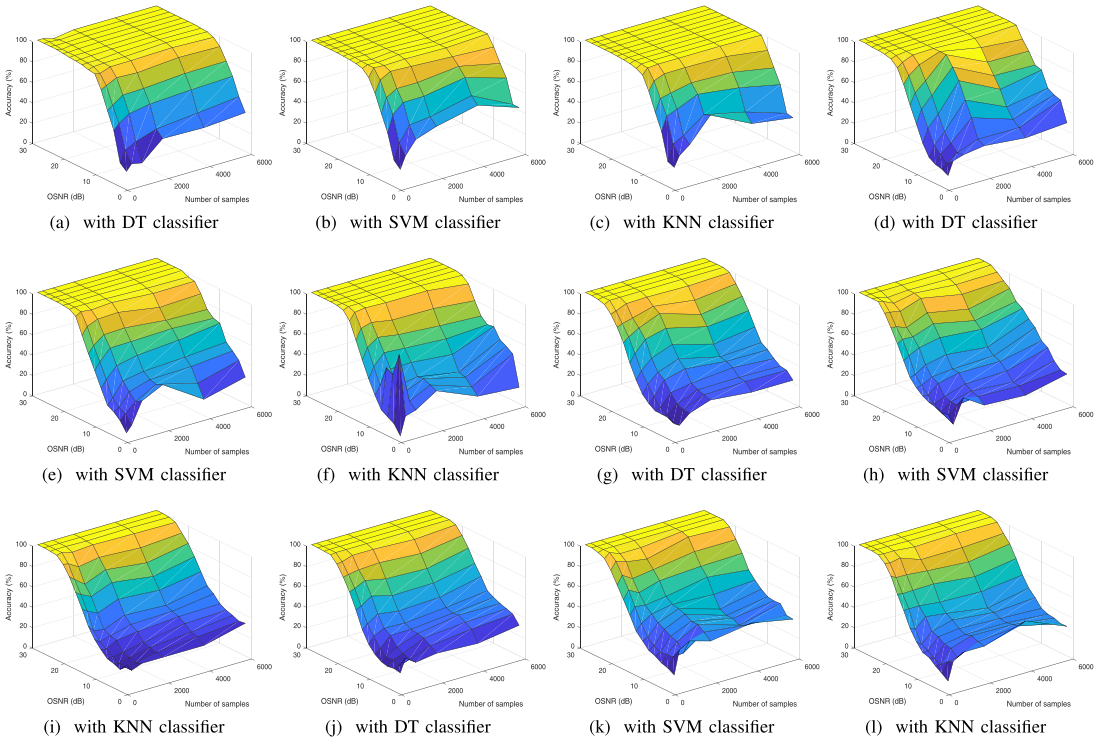

(a) with DT classifier (b) with SVM classifier (c) with KNN classifier (d) with DT classifier

(e) with SVM classifier (f) with KNN classifier (g) with DT classifier (h) with SVM classifier

(i) with KNN classifier (j) with DT classifier (k) with SVM classifier (l) with KNN classifier

Fig. 11. Accuracy vs. number of samples and OSNR values for all QAM modulation formats with the SVD scheme. (a), (b), (c) are for 4-QAM; (d), (e), (f) are for 16-QAM; (g), (h), (i) are for 64-QAM; and (j), (k), (l) are for 256-QAM.

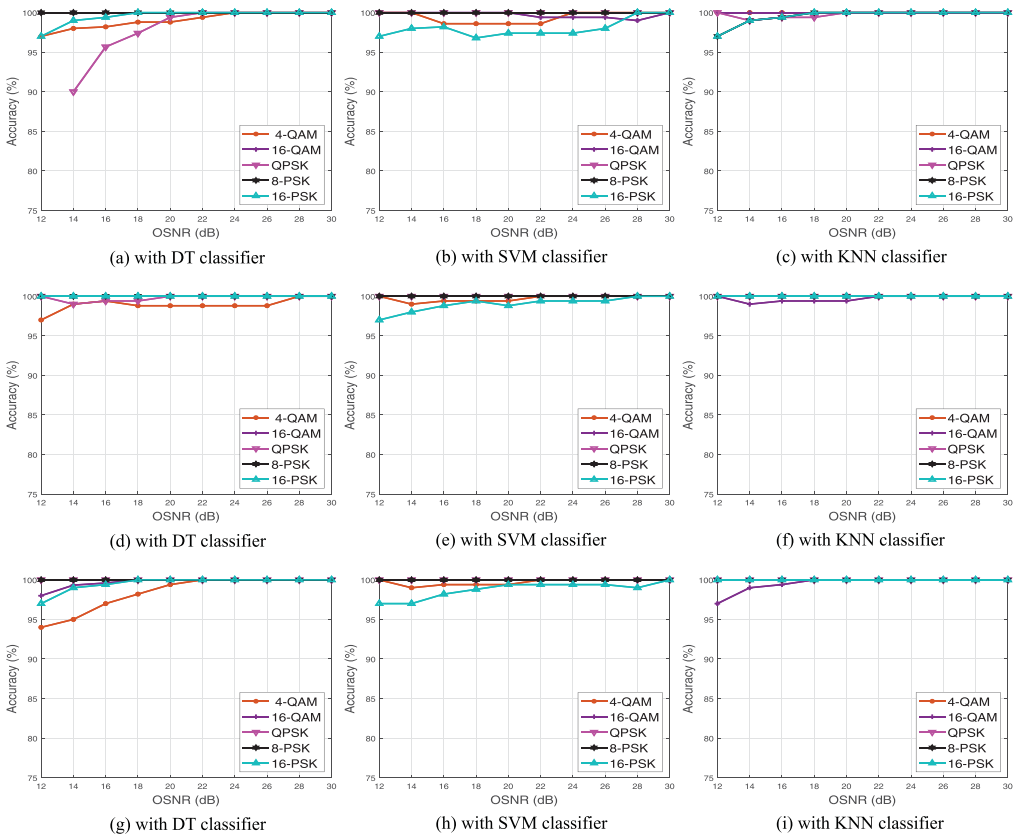

(a) with DT classifier (b) with SVM classifier (c) with KNN classifier

(d) with DT classifier (e) with SVM classifier (f) with KNN classifier

(g) with DT classifier (h) with SVM classifier (i) with KNN classifier

Fig. 12. Accuracy vs. OSNR for all modulation formats with SVD scheme for all used samples for Opti-System constellation. (a), (b), (c) are with 250 samples; (d), (e), (f) are with 500 samples; and (g), (h), (i) are with 1000 samples.

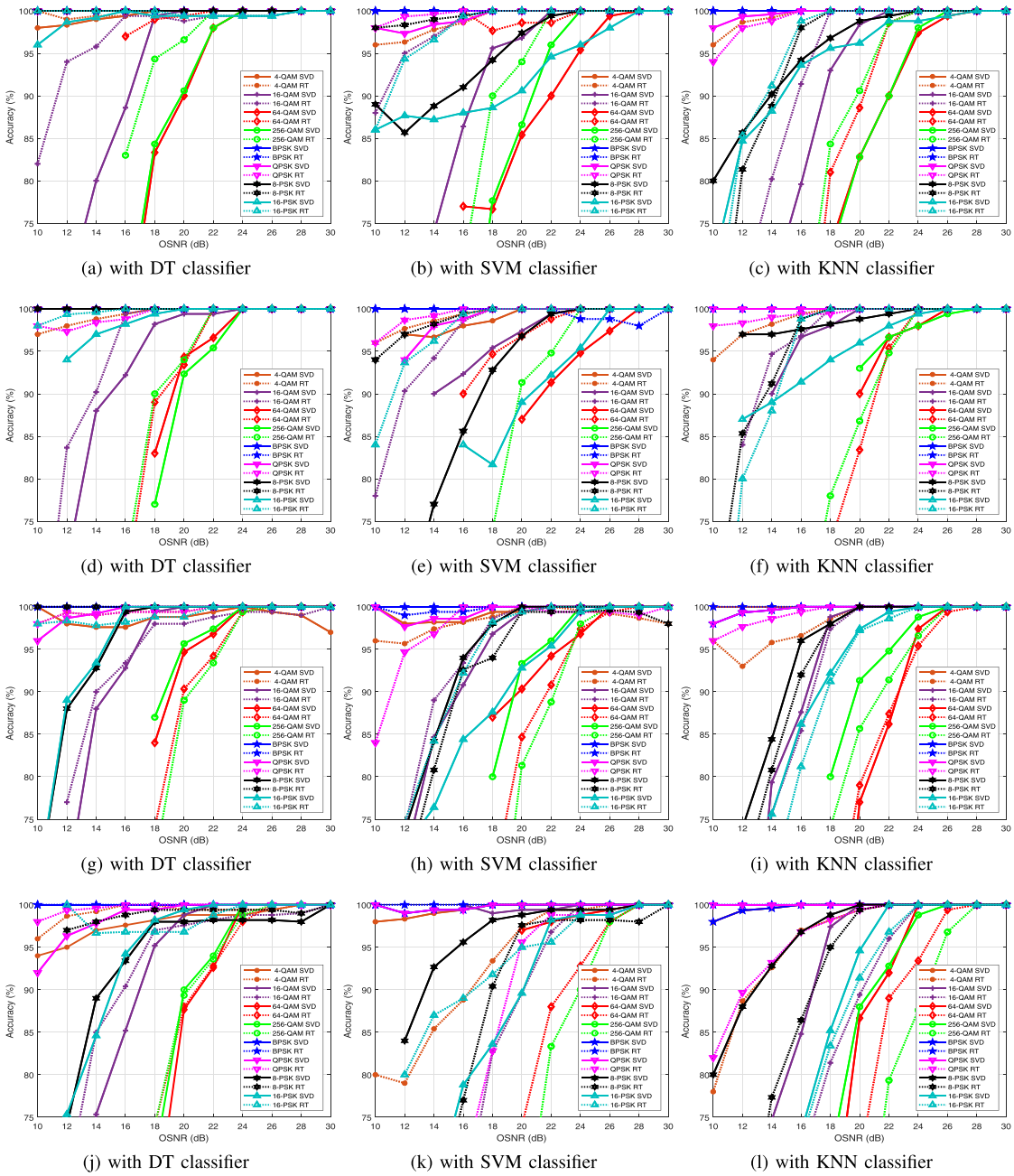

(a) with DT classifier (b) with SVM classifier (c) with KNN classifier

(d) with DT classifier (e) with SVM classifier (f) with KNN classifier

(g) with DT classifier (h) with SVM classifier (i) with KNN classifier

(j) with DT classifier (k) with SVM classifier (l) with KNN classifier

Fig. 13. Accuracy vs. OSNR for all modulation formats with both RT and SVD scheme and SVD scheme only for all used samples. (a), (b), (c) are with 6000 samples; (d), (e), (f) are with 4000 samples; (g), (h), (i) are with 1000 samples; and (j), (k), (l) are with 500 samples.

5° to 45° with 10° steps. The two proposed schemes are applied and tested with the DT and KNN classifiers.

VII. Experimental Setup

To ensure the feasibility of the two proposed (SVD and SVD with RT) schemes in MFI for optical transmission systems, a proof-of-concept experiment is conducted using the setup shown in Fig. 7. A continuous-wave distributed feedback (DFB) fiber laser (NKTPhotonics Koheras Adjustic) operating at 1550 nm with an output power of 15 dBm is applied to a dual-polarization Mach-Zehnder modulator (DP-MZM) (Fujitsu FTM7977HQA). The DP-MZM has a switching voltage of 4.6 volts and an insertion loss of 7 dBs. A four channel 64 GSa/s arbitrary waveform generator (AWG) (Keysight M9185 A) is used to generate pseudo-random binary sequences (PRBS-11) that are coded into multi-level IQ signals. In particular, the generated modulation pool includes three DP-formats: DP-4-QAM, DP-16-QAM and DP-64-QAM. The OSNR values are adjusted using Amonics Erbium-doped fiber amplifier (AEDFA-C-18B-R) that generates an amplified spontaneous emission noise (ASE) controlled by a tunable optical attenuator (OA). A 50:50 optical coupler (OC) is used to couple the signal and the ASE noise. The received modulated optical signal is coherently detected and digitized

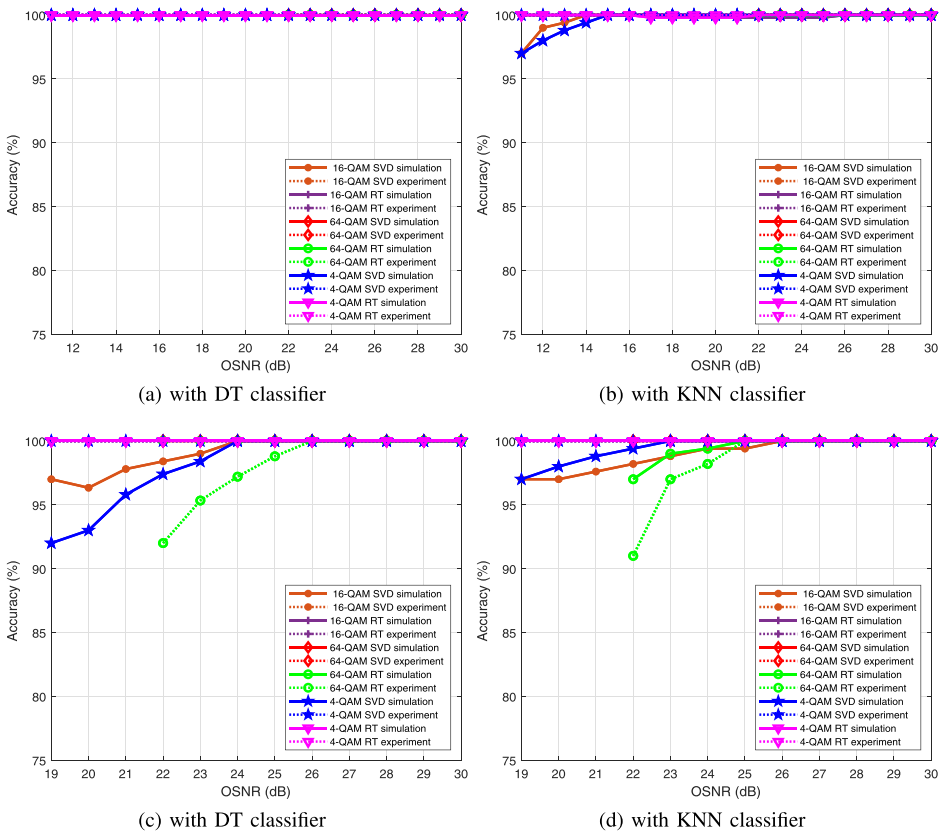

(a) with DT classifier (b) with KNN classifier

(c) with DT classifier (d) with KNN classifier

Fig. 14. Accuracy vs. OSNR for the three dual-polarized modulation formats with both RT and SVD scheme and SVD only with 1000 samples. (a), (b) are at 100 kHz and (c), (d) are at 1 MHz PN with the experimental and simulation constellation diagrams.

using Keysight digital storage oscilloscope (DSOX93294 A). The stored samples are offline-processed, where the feature extraction using the proposed schemes is applied. Then, the modulation formats are identified using the KNN or DT classifiers.

The experimental work is compared with a simulation setup at variable bit rates for three dual-polarized modulation formats: 20 Gbps-DP-4-QAM, 40 Gbps-DP-16-QAM and 60 Gbps-DP-64-QAM. The PN is considered for the three formats, with values of 1, 10, 100 and 1000 kHz. The OSNR is controlled to be variable from 11 to 30 dB for the three modulation formats. The front-end compensation, CD compensation and clock recovery can be performed before the MFI step, as they are modulation format independent DSP processes [5], [8], [12]. The used three formats are square modulation, which leads to providing a standard step size for the adaptive equalization. This makes the proposed MFI usable before the adaptive equalization.

VIII. Results and Discussion

Figs. 8 to 16 present the simulation and experimental results. Different numbers of samples are used in the setup at various OSNR values. At each observation with certain number of samples and OSNR value, fifty constellation diagrams are collected for each format. Fig. 8 shows examples of the simulation results of accuracy versus OSNR with the three selected classifiers with 4000 samples. It is clear from the figure that the accuracy of classification is different for each modulation. For the eight used modulation formats, the DT and KNN classifiers are better than the SVM classifier even with the higher order modulation formats.

Fig. 9 clarifies the effect of using the proposed hybrid scheme of RT and SVD on the classification rates compared to the SVD only. The utilization of the RT enhances the accuracy for all modulation formats at low OSNR values even for higher-order modulation formats. It is obvious that the DT and KNN classifiers achieve the highest accuracies with the RT and SVD scheme. Additionally, 16-QAM, 64-QAM, 256-QAM and BPSK achieve higher accuracy levels with all classifiers, but 4-QAM, QPSK, 8-PSK and 16-PSK achieve better accuracy levels with the DT and KNN classifiers.

Furthermore, 3D graphs showing the variation of the accuracy with both the number of samples and the OSNR are given in Figs. 10 and 11 for all formats with the SVD scheme only. Fig. 10 depicts the 3D graphs for all PSK modulation orders. It shows that the accuracy level is above 98% at different OSNR values with definite classifiers for PSK modulation. For BPSK, there is a need for an OSNR value above 6 dBs with all numbers of samples and all classifiers to achieve accuracy levels above 98%. QPSK modulation achieves accuracy levels above 98% beginning from 8 dBs with the DT and KNN classifiers. For the SVM classifier, 10 dBs are required. To achieve high classification rates for 8-PSK, 12 dBs are required with the DT classifier, 14 dBs with the KNN classifier

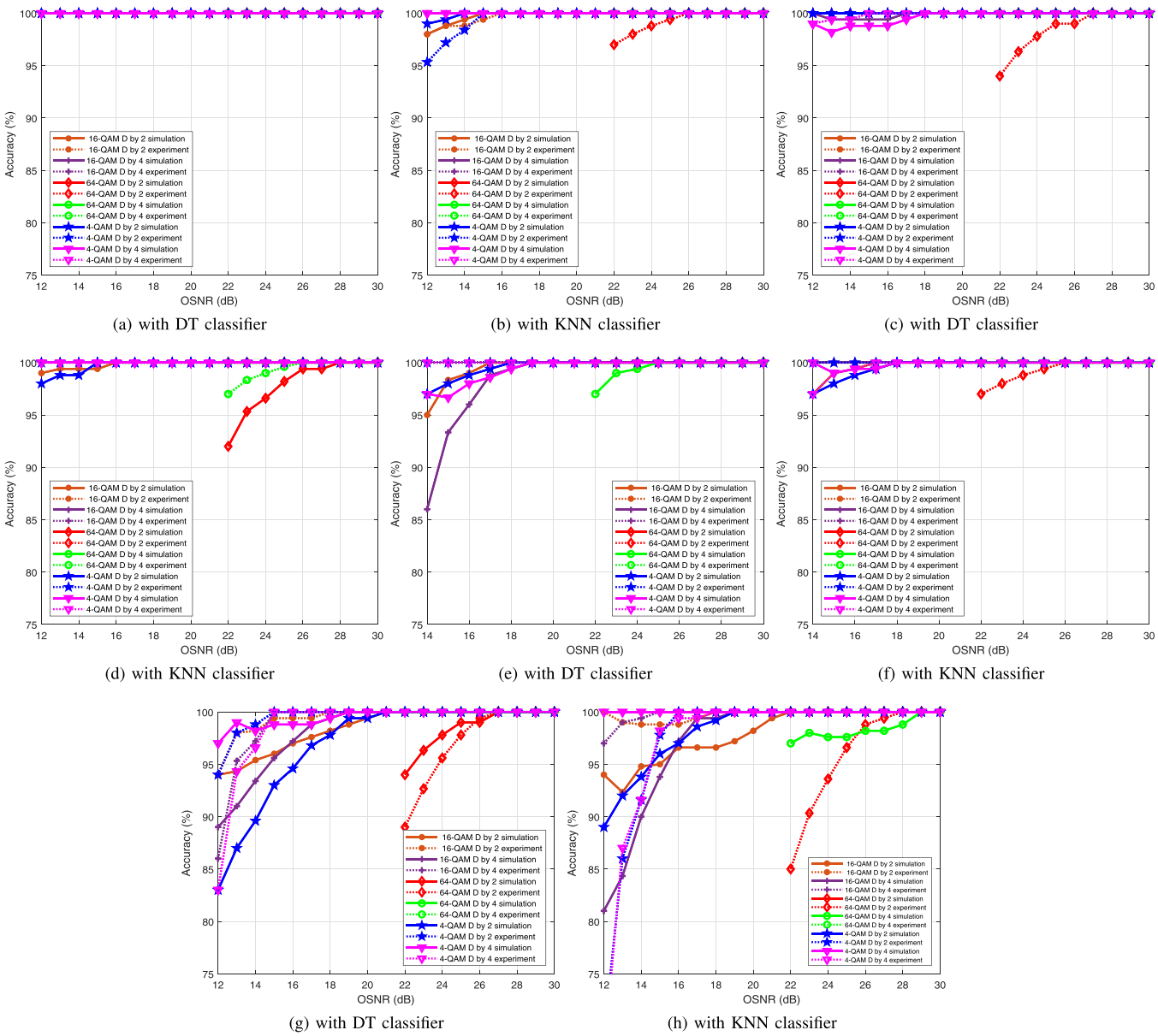

(a) with DT classifier (b) with KNN classifier (c) with DT classifier

(d) with KNN classifier (e) with DT classifier (f) with KNN classifier

(g) with DT classifier (h) with KNN classifier

Fig. 15. Accuracy vs. OSNR for the three dual-polarized modulation formats for decimation by 2 and 4 with SVD scheme with 1000 samples. (a), (b) are at 1 kHz; (c), (d) are at 10 kHz; (e), (f) are at 100 kHz; and (g), (h) are at 1 MHz with the experimental and simulation constellation diagrams.

and 16 dBs with the SVM classifier. Additionally, obtaining high accuracy levels above 98% for 16-PSK requires 14 dBs with the KNN and SVM classifiers and 12 dBs with the DT classifier.

Fig. 11 presents the 3D graphs for all used QAM modulation formats. The accuracy is above 98% at definite values of the OSNR for each classifier. For 4-QAM, a 10-dB OSNR is required with all classifiers. Moreover, 16-QAM needs 16 dBs with the SVM and KNN classifiers to achieve accuracy levels above 99% and 14 dBs with the DT classifier for the same objective. For 64-QAM, 20 dBs are required with the DT classifier, but 22 dBs are required with the KNN classifier and 24 dBs with the SVM classifier to get accuracy levels above 99%. For 256-QAM, 20 dBs are required with the DT classifier, and 22 dBs with the SVM and KNN classifiers to provide accuracy levels above 99%.

Fig. 12 shows the accuracy versus OSNR for modulation formats generated from Opti-System simulation. It is clear that the accuracy of classification is better with all used classifiers, especially with large numbers of samples, but with small numbers of samples, the DT and KNN classifiers are better than the SVM classifier.

Fig. 13 presents a comparison between the SVD scheme and the RT with SVD scheme for all numbers of samples. As shown in the figure, the RT with SVD scheme enhances the MFI performance at low OSNR values for higher-order modulation formats down to 1000 samples. The performance enhancement with the RT with SVD scheme is attributed to the robustness of the RT and the stability of the SVD to constellation diagram variations. In the generation of constellation diagrams, the presence of impairments is possible. So, there is a need to use impairment-robust decomposition techniques.

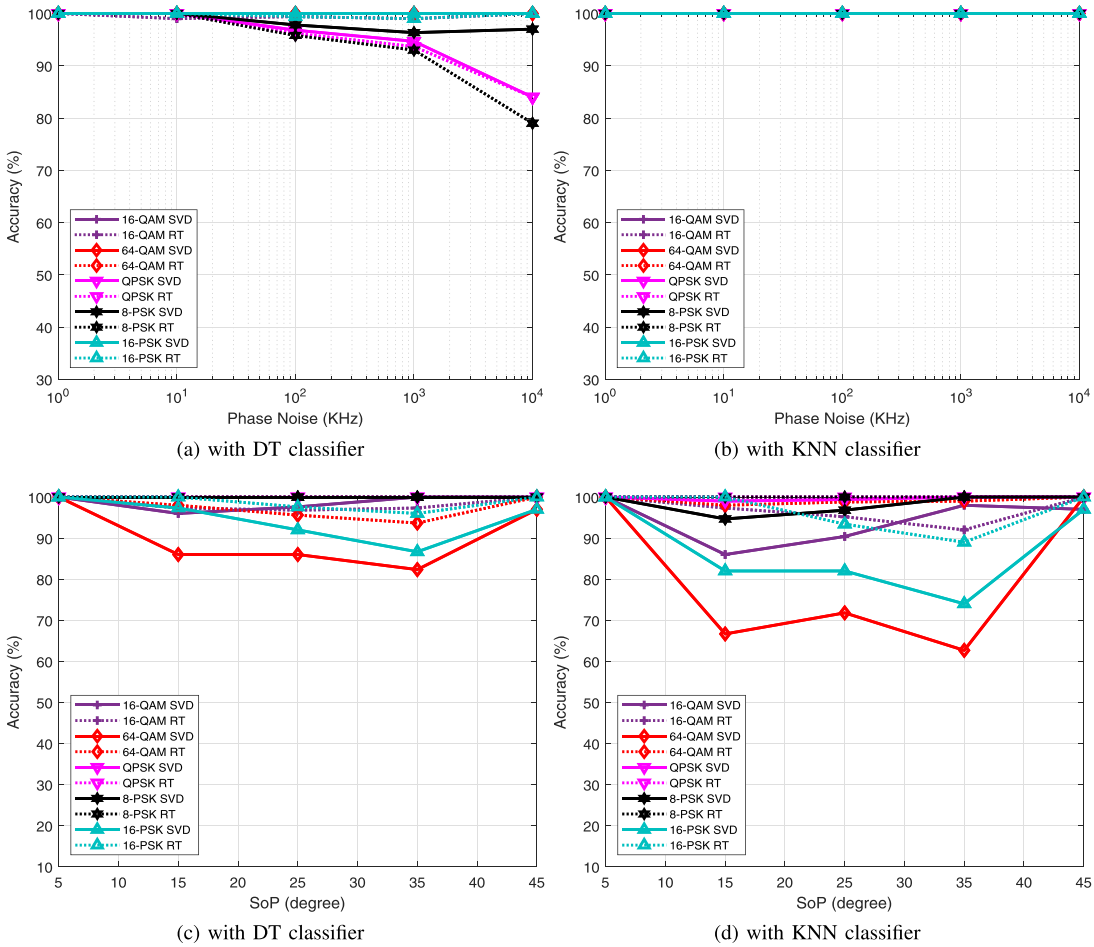

(a) with DT classifier (b) with KNN classifier

(c) with DT classifier (d) with KNN classifier

Fig. 16. Accuracy vs. PN or SoP for the five dual-polarized modulation formats with both RT and SVD scheme and SVD scheme only with 1000 samples. (a), (b) are at all used PN values and (c), (d) are at all SoP values with the simulation constellation diagrams.

Finally, we present simulation and experimental results for the 20 Gbps-DP-4-QAM, 40 Gbps-DP-16-QAM and 60 Gbps-DP-64-QAM formats with the DT and KNN classifiers. The obtained results show that for the lower levels of PN (1 and 10 kHz), the identification accuracy reaches 100% for the three formats at an OSNR greater than 11 dBs.

Fig. 14 provides the accuracy versus OSNR for the two proposed schemes. For DP-4-QAM, the RT shows the best performance at all PN levels with both classifiers. Also, the SVD scheme achieves a high accuracy level but with 1 MHz, 23 dBs for the KNN classifier and 24 dBs for the DT classifier are required. For DP-16-QAM, 24 dBs and 26 dBs are required with the DT and KNN classifiers, respectively, to provide 100% accuracy levels at 1 MHz. For DP-64-QAM, 25 dBs and 26 dBs are required with the KNN and DT classifiers to reach 100% accuracy levels at 1 MHz, respectively.

Fig. 15 presents the accuracy with the decimation process for the SVD scheme. It is shown that the variation in accuracy is not significant up to 100 kHz, while at 1 MHz, higher OSNRs are required to reach a 100% accuracy.

The 100% recognition accuracy achieved at relatively high OSNRs is intuitively not surprising, because the RT images have distinguishable shapes even at 1 MHz, as demonstrated in Fig. 4 for OSNR = 30 dBs. Note that the phase-noise-induced rotation is not a common rotation to all points in a constellation diagram, but a symbol-by-symbol rotation, resulting in a circle-like constellation diagram. Therefore, for high values of PN, the proposed schemes may find difficulty to identify M-PSK modulation formats. Fig. 4 shows the constellation diagrams and their RTs at OSNR = 30 dBs revealing some degradations.

It is relevant to mention here that RT images have also distinguishable shapes in the presence of polarization cross-talk, which leads to relatively high recognition accuracy. This can be justified from the samples of RT images for polarization-crosstalk presented in Fig. 5. Fig. 16 shows the accuracy versus PN levels of 1 kHz, 10 kHz, 100 kHz, 1 MHz and 10 MHz and polarization cross-talk with rotation angles of 5, 15, 25, 35 and 45°.

The recognition rate has been studied versus the level of PN and SoP values with the two proposed schemes using different types of classifiers. The results shown in Fig. 16 reveal that the proposed schemes with the selected classifiers (DT and KNN) can resist the effects of PN and polarization cross-talk.

A simple comparison is provided between the proposed schemes and the previous works, depending on the number of

TABLE I
REQUIRED OSNR AND NUMBER OF SAMPLES TO GET 100% ACCURACY

	16-QAM	BPSK	QPSK	8-PSK	16-PSK
Proposed SVD scheme	14 dBs with 2000	8 dBs with 1000	10 dBs with 500	14 dBs with 2000	16 dBs with 2000
Scheme in [5]	16.5 dBs with 10000	–	11.2 dBs with 10000	–	–
Scheme in [9]	22 dBs with 10000	–	12 dBs with 4000	22 dBs with 4000	–
Scheme in [20]	19.5 dBs with 5000	9 dBs with 1000	11.5 dBs with 3000	13 dBs with 3000	16.5 dBs with 3000
Scheme in [21]	7 dBs with 400000	7 dBs with 400000	7 dBs with 400000	7 dBs with 400000	–

samples and OSNR values that provide high accuracies of 100%. We have used OSNR values of 12, 19, and 24 dBs for 4, 16, and 64-QAM, respectively, as in [19]. When compared to that of [19], the proposed SVD scheme requires less samples for the same modulation formats. Specifically, it requires 250, 500, and 250 samples for 4, 16, and 64-QAM, respectively, while 500, 5500, and 1000 samples are needed in [19], respectively.

Moreover, a comparison between previous schemes for blind MFI and the proposed SVD scheme is given in Table I. It is shown that there is a need for a trade-off between the required OSNR value and the number of samples to achieve a 100% accuracy level. The proposed schemes provide blind MFI at lower OSNR values and less samples for all modulation formats compared to the other schemes.

Specifically, for 16-PSK, the proposed SVD scheme needs 16 dBs with 2000 samples to reach a 100% accuracy, but in [20], 16.5 dBs are required with 3000 samples to achieve the same accuracy level. In addition, the higher-order QAM modulation formats are considered in the comparison. The proposed SVD scheme requires an OSNR of 24 dBs with 4000 samples for 64-QAM and 256-QAM to achieve a 100% classification accuracy, while 24 dBs and 31 dBs with 10000 samples are required to classify 64-QAM and 256-QAM, respectively, in [5].

IX. CONCLUSION

A new trend in optical MFI based on constellation diagram analysis has been proposed and examined using simulation and experimental demonstrations. This analysis is performed either through the extraction of the SVs directly from the constellation diagrams or through the extraction of the SVs from RTs of these diagrams to constitute the feature vectors. The inherent stability characteristics of SVs in the presence of matrix perturbations are well exploited to yield high accuracy of MFI. In addition, the outstanding characteristic of the RT that guarantees stability to impairment effects is well exploited to yield high accuracy levels, even with high-order modulation formats at low OSNR values with as less samples as possible. The decimation process provides a reduction in the complexity of SVD computations, while keeping 100% accuracy levels. The efficiency of the two proposed schemes with the PN and SoP effects has been verified for the used modulation formats. Different classifiers have been tested and compared for the MFI purpose. We can conclude that the SVM, DT and KNN classifiers are excellent candidates to build a robust MFI system based on the RT and the SVD.

REFERENCES

[1] A. Nag, M. Tornatore, and B. Mukherjee, "Optical network design with mixed line rates and multiple modulation formats," *J. Lightw. Technol.*, vol. 28, no. 4, pp. 466–475, Feb. 2009.

[2] Z. Zhu and A. K. Nandi, *Automatic Modulation Classification: Principles, Algorithms and Applications.* Hoboken, NJ, USA: Wiley, 2014.

[3] S. M. Bilal, G. Bosco, Z. Dong, A. P. T. Lau, and C. Lu, "Blind modulation format identification for digital coherent receivers," *Opt. Express*, vol. 23, no. 20, pp. 26769–26778, 2015.

[4] E. J. Adles *et al.*, "Blind optical modulation format identification from physical layer characteristics," *J. Lightw. Technol.*, vol. 32, no. 8, pp. 1501–1509, Apr. 2014.

[5] J. Liu, Z. Dong, K. Zhong, A. P. T. Lau, C. Lu, and Y. Lu, "Modulation format identification based on received signal power distributions for digital coherent receivers," in *Proc. Opt. Fiber Commun. Conf.*, 2014, Paper Th4D–3.

[6] F. Musumeci *et al.*, "An overview on application of machine learning techniques in optical networks," *IEEE Commun. Surv. Tut.*, vol. 21, no. 2, pp. 1383–1408, Secondquarter 2019.

[7] F. N. Khan, Y. Zhou, A. P. T. Lau, and C. Lu, "Modulation format identification in heterogeneous fiber-optic networks using artificial neural networks," *Opt. Express*, vol. 20, no. 11, pp. 12422–12431, 2012.

[8] F. N. Khan, K. Zhong, W. H. Al-Arashi, C. Yu, C. Lu, and A. P. T. Lau, "Modulation format identification in coherent receivers using deep machine learning," *IEEE Photon. Technol. Lett.*, vol. 28, no. 17, pp. 1886–1889, Sep. 2016.

[9] T. Bo, J. Tang, C.-K. Chan, and C. Chun-Kit, "Blind modulation format recognition for software-defined optical networks using image processing techniques," in *Proc. Opt. Fiber Commun. Conf. Exhib.*, 2016, pp. 1–3.

[10] J. Zhange, W. Chen, M. Gao, Y. Ma, Y. Zhao, and G. Shen, "Intelligent adaptive coherent optical receiver based on convolutional neural network and clustering algorithm," *Opt. Express*, vol. 26, no. 14, pp. 18684–18698, 2018.

[11] D. Wang *et al.*, "Intelligent constellation diagram analyzer using convolutional neural network-based deep learning," *Opt. Express*, vol. 25, no. 15, pp. 17150–17166, 2017.

[12] D. Wang *et al.*, "Modulation format recognition and OSNR estimation using CNN-based deep learning," *IEEE Photon. Technol. Lett.*, vol. 29, no. 19, pp. 1667–1670, Oct. 2017.

[13] F. E. Abd El-Samie, *Information Security for Automatic Speaker Identification.* Berlin, Germany: Springer, 2011.

[14] S. Kolouri, S. R. Park, and G. Rohde, "The Radon cumulative distribution transform and its application to image classification," *IEEE Trans. Image Process.*, vol. 25, no. 2, pp. 920–934, Feb. 2016.

[15] T. Pfau, S. Hoffmann, and R. Noé, "Hardware-efficient coherent digital receiver concept with feedforward carrier recovery for M-QAM constellations," *J. Lightw. Technol.*, vol. 27, no. 8, pp. 989–999, Apr. 2009.

[16] J. Yu and J. Zhang, "Recent progress on high-speed optical transmission," *Digit. Commun. Netw.*, vol. 2, no. 2, pp. 65–76, 2016.

[17] J. H. Shin, J. H. Jung, and J. K. Paik, "Regularized iterative image interpolation and its application to spatially scalable coding," *IEEE Trans. Consum. Electron.*, vol. 44, no. 3, pp. 1042–1047, Aug. 1998.

[18] O. Fontenla-Romero, B. Pérez-Sánchez, and B. Guijarro-Berdiñas, "LANN-SVD: A non-iterative SVD-based learning algorithm for one-layer neural networks," *IEEE Trans. Neural Netw. Learn. Syst.*, vol. 29, no. 8, pp. 3900–3905, Aug. 2018.

[19] X. Lin, Y. A. Eldemerdash, O. A. Dobre, S. Zhang, and C. Li, "Modulation classification using received signals amplitude distribution for coherent receivers," *IEEE Photon. Technol. Lett.*, vol. 29, no. 21, pp. 1872–1875, Nov. 2017.

[20] L. Jiang *et al.*, "Blind density-peak-based modulation format identification for elastic optical networks," *J. Lightw. Technol.*, vol. 36, no. 14, pp. 2850–2858, Jul. 2018.
[21] G. Liu, R. Proietti, K. Zhang, H. Lu, and S. B. Yoo, "Blind modulation format identification using nonlinear power transformation," *Opt. Express*, vol. 25, no. 25, pp. 30895–30904, 2017.

Rania A. Eltaieb was born in Sohag, Egypt, in 1993. She received the B.Sc. degree (with Hons.) from Menoufia University, Menouf, Egypt, in 2016, where she is currently working toward the M.Sc. degree with the Electronics and Electrical Communications Engineering Department. In 2017, she joined the Electronics and Electrical Communications Engineering Department, Menoufia University as a Teaching Assistant. Her research interests include digital communications, optical signal processing, optical modulation format identification, image processing, and machine learning.

Ahmed E. A. Farghal received the B.Sc. (with Hons.) and M.Sc. degrees from Menoufia University, Menoufia, Egypt, and the Ph.D. degree from Egypt-Japan University for Science and Technology, Alexandria, Egypt, all in electrical engineering, in 2006, 2011, and 2015, respectively. In 2007, he joined the Department of Electronics and Electrical Communications Engineering, Faculty of Electronic Engineering, Menoufia University, and was promoted to the position of a Lecturer Assistant in 2011. From November 2014 to July 2015, he joined Kyushu University, Fukuoka, Japan, as a Special Research Student. He was with the Department of Electronics and Electrical Communications Engineering, Faculty of Electronic Engineering, Menoufia University, where he was an Assistant Professor. He is currently with the Electrical Engineering Department, Faculty of Engineering, Sohag University, Sohag, Egypt. His research interests include optical CDMA, all-optical networks, QoS provisioning in optical networks, elastic optical networking, green optical networks, and nano-optoelectronic devices.

HossamEl-din H. Ahmed received the B.Sc. degree (Hons) in nuclear engineering in June 1969, the M.Sc. degree in microelectronic electron diffraction from the Nuclear Department, Faculty of Engineering, Alexandria University, Alexandria, Egypt, in 1977, and the Ph.D. degree from the High Institute of Electronics and Optics, Paul Sabatier University, Toulouse, France, in 1983. From 1970 to 1977, he was in the Egyptian Marine Force. He was a demonstrator until 1977. In 1977, he was a Teaching Lecturer and a Staff Member. In 1993, he was a Professor with the Department of Electronics and Electrical Communications Engineering, Faculty of Electronic Engineering, Menoufia University, Egypt. From 1993 to 1999, he was a Vice Dean for Educations and Students Affairs. In 2001, he became the Head of the Electrical Communications Department. From 2001 to 2004, he was the Dean of the Faculty of Electronic Engineering. He is a member of the *Menoufia Periodic Electronic Journal*, and since 1995 he has been the Director, Designer, and Constructor of the Menoufia University wide-area network (WAN) (21-LANs). He is the developer of the Menoufia University libraries and FRCU universities libraries in Egypt. His current research interests are electron and scan microscopy, transmission and backscattering of electrons and ion beams into amorphous or polycrystalline targets, optical fibers, VLSI design, nanotechnology, lithography, digital, optical, and multimedia communications, digital image processing, computer security (crypto-analysis), telemetry microcomputer applications in satellites, satellite communications, IT, and computer networks.

Waddah S. Saif received the B.Sc. degree in communications engineering from Hadhramout University, Hadhramout, Yemen, in 2003, and the M.S. degree in electrical engineering from King Saud University, Riyadh, Saudi Arabia, in 2015, where he is currently working toward the Ph.D. degree with the Electrical Engineering Department. His research interests include optical communications and machine learning.

Amr Ragheb received the B.S. (Hons.) and M.Sc. degrees from Tanta University, Tanta, Egypt, in 2001 and 2007, respectively, and the Ph.D. degree from King Saud University, Riyadh, Saudi Arabia, in 2015, all in electrical engineering. He was a Teaching Assistant (TA) with Tanta University, Egypt, from 2003 to 2008. He was a TA with King Saud University, from 2010 to 2015. He has more than seven years of experience with Photonics Telecommunication Laboratory. He is currently an Assistant Professor with King Saud University. He has contributed to the research areas, such as photonic-microwave integration, quantum dash-based lasers, free-space optical communications, optical modulation format identification, coherent optical receivers, multi-format high-speed optical transmitter, and passive optical networks.

Saleh A. Alshebeili was the Chairman with the Electrical Engineering Department, King Saud University, Riyadh, Saudi Arabia from 2001 to 2005. He has more than 27 years of teaching and research experience in the area of communications and signal processing. He was a member of the Board of Directors with the King Abdullah Institute for Research and Consulting Studies, from 2007 to 2009, a member of the Board of Directors with Prince Sultan Advanced Technologies Research Institute, from 2008 to 2017, where he was the Managing Director from 2008 to 2011, and the Director of the Saudi-Telecom Research Chair from 2008 to 2012. He has been the Director of the Technology Innovation Center, RF and Photonics in e-Society, funded by the King Abdulaziz City for Science and Technology (KACST), since 2011. He is currently a Professor with Electrical Engineering Department, King Saud University. He has been in the Editorial Board of the Journal of Engineering Sciences of King Saud University from 2009 to 2012. He has also an active involvement in the review process of a number of research journals, KACST general directorate grants programs, and national and international symposiums and conferences.

Hossam M. H. Shalaby (S'83–M'91–SM'99) was born in Giza, Egypt, in 1961. He received the B.S. and M.S. degrees from Alexandria University, Alexandria, Egypt, in 1983 and 1986, respectively, and the Ph.D. degree from the University of Maryland, College Park, MD, USA, in 1991, all in electrical engineering. In 1991, he joined Electrical Engineering Department with Alexandria University, and was promoted to a Professor in 2001. Since November 2017, he has been on leave from Alexandria University, where he is a Professor with the Department of Electronics and Communications Engineering (ECE), School of Electronics, Communications, and Computer Engineering, Egypt-Japan University of Science and Technology (E-JUST), Alexandria. From September 2010 to August 2016, he was the Chair with the ECE Department, E-JUST. From December 2000 to 2004, he was an Adjunct Professor with the Faculty of Sciences and Engineering, Department of Electrical and Information Engineering, Laval University, Quebec, QC, Canada. From September 1996 to January 1998, he was with the Electrical and Computer Engineering Department, International Islamic University, Malaysia, and from February 1998 to February 2001, he was with the School of Electrical and Electronic Engineering, Nanyang Technological University, Singapore. He was a Consultant at SysDSoft company, Alexandria, from 2007 to 2010. His research interests include optical communications, silicon photonics, optical CDMA, and quantum information theory. He was a student branch counselor with Alexandria University, IEEE Alexandria, and North Delta Subsection, from 2002 to 2006, and was a Chairman of the student activities committee of IEEE Alexandria Subsection from 1995 to 1996. He was the recipient of an SRC fellowship from 1987 to 1991 from Systems Research Center, Maryland, State Excellence Award in Engineering Sciences in 2007 from the Academy of Scientific Research and Technology, Egypt, Shoman Prize for Young Arab Researchers in 2002 from the Abdul Hameed Shoman Foundation, Amman, Jordan, State Incentive Award in Engineering Sciences in 1995 and 2001 from the Academy of Scientific Research and Technology, Egypt, University Excellence Award in 2009 from Alexandria University, and University Incentive Award in 1996 from Alexandria University. He is a Senior Member of the IEEE Photonics Society and The Optical Society of America.

Fathi E. Abd El-Samie received the B.Sc. (Hons.), M.Sc., and Ph.D. degrees from Menoufia University, Menouf, Egypt, in 1998, 2001, and 2005, respectively. Since 2005, he has been a Teaching Staff Member with the Department of Electronics and Electrical Communications, Faculty of Electronic Engineering, Menoufia University. His current research interests include image enhancement, image restoration, image interpolation, super-resolution reconstruction of images, data hiding, multimedia communications, medical image processing, optical signal processing, and digital communications. He was the recipient of the Most Cited Paper Award from the *Digital Signal Processing Journal* in 2008.